Available online at www.sciencedirect.com
SCIENCE DIRECT
NDT&E International 38 (2005) 359–367
NDT&E international
www.elsevier.com/locate/ndteint

Measurement of the electrical conductivity of open-celled aluminium foam using non-contact eddy current techniques

X. Ma[a,*], A.J. Peyton[a], Y.Y. Zhao[b]

[a]*Engineering Department, Lancaster University, Lancaster LA1 4YR, UK*
[b]*Department of Engineering, University of Liverpool, Liverpool L69 3GH, UK*

Received 10 September 2004; revised 5 October 2004; accepted 11 October 2004
Available online 2 December 2004

Abstract

This paper studies the electrical properties of open-celled aluminium foams manufactured by a novel sintering-dissolution process (SDP) using non-destructive eddy current testing. Experimental measurement results are first presented by means of an impedance analyser under swept frequency testing for the determination of electrical conductivity of Al foams. A double air-cored solenoidal sensor has been constructed for the purpose of evaluating cylindrically shaped samples used in the investigations. The effects of porosity (relative density) and pore size, which are the principle parameters of the foams, on the conductivity are examined. The results demonstrate that the electrical conductivity of Al foam is strongly dependent on both porosity and pore size. The sensor geometry is further simulated electromagnetically using finite element methods, by which the mutual impedance between two coils is calculated to solve the forward electromagnetic (EM) induction problem to provide a calibration curve relating the mutual impedance change with the electrical conductivity of the sample. The results obtained from experimental measurements are found to be in good quantitative agreement with the finite element simulations.

Keywords: Eddy currents; Conductivity; Impedance; Metallic foams; Finite element modelling

1. Introduction

Over recent years, the exceptional combination of mechanical, thermal, acoustic, electrical and chemical properties of aluminium foams has increasingly been recognized. This has led to a variety of potential industrial applications for this relatively new type of material, particularly in the areas of energy absorption, thermal and acoustic management, and lightweight structures for transport and architecture. Manufacturing methods of Al foams can be classified in terms of the Al precursory forms and the types of the pore-forming agents utilized. The main classes include melt-gas injection, melt-foaming agents, powder-foaming agents, pressure infiltration and sintering-dissolution process. Compared to other manufacturing methods, the sintering-dissolution process (SDP) is a relatively cost effective manufacturing technology as it exploits inexpensive raw materials and simple process equipment. It also allows the shape of the pores to be controlled. The process starts by mixing Al and NaCl powders thoroughly at a pre-specified volume ratio, after which the mix is compacted into a net-shape preform under an appropriate pressure. The resulting preform is sintered at a temperature around the melting point of Al, thus allowing Al to form a well-bonded network structure, which is then cooled to room temperature. An open cell aluminium foam is finally attained by dissolving the imbedded NaCl in water. Detailed descriptions of the SDP method are given elsewhere [1,2].

To allow an industrial application of aluminium foams, evaluation of the foam properties is necessary. Of these, the electrical properties of Al foams are of paramount interest, which requires non-destructive measurement to characterise the foam structure. Eddy current testing is attractive because it is non-destructive and non-invasive in nature. This enables improved understanding of the foam properties, its processing and hence the ability to control its properties through characterising the electrical properties. The eddy current technique has been proven over several decades to be well

* Corresponding author. Tel.: +44 1524 593326; fax: +44 1524 381707.
E-mail address: x.ma@lancaster.ac.uk (X. Ma).

0963-8695/$ - see front matter © 2004 Elsevier Ltd. All rights reserved.
doi:10.1016/j.ndteint.2004.10.003

suited for non-destructive material property evaluation and inspection [3,4], particularly in harsh production environments, e.g. monitoring the Bridgman crystal growth [5] and more recently imaging the molten steel flow profiles [6,7]. The application of eddy current testing to metal foams is relatively new and very limited information has been documented in this respect to date. Apparently, the electromagnetic sensor outputs are affected significantly by the foam's relative density and its macrostructures due to the amount of the volume of metal aluminium within the foam and the tortuosity of the current path. Measurement of the impedance change in the sensor coil(s) permits the metal foams to be characterised by correlating the coil impedance change to the characteristic quantities of interest. An earlier report [8] demonstrated that the relative density and pore size could be differentiated qualitatively in terms of the measured impedance change through the electrical impedance measurements on the Al foams.

This paper focuses on the evaluation of open-celled aluminium foams produced using the SDP method in order to measure the equivalent electrical conductivity via electromagnetic sensor coils. Experimental measurement results are first presented, which were obtained with impedance analyser and swept frequency testing for the determination of electrical conductivity of Al foams. Of common interests in the investigations are the effects of porosity (relative density) and macrostructures such as pore size on the electrical conductivity of the foams. The air-cored sensor coils were employed to test the cylindrically shaped samples used in the investigations. The phase signature of the sensor output has been shown to be radius invariance [9,10], by which the electrical conductivity of the foams can be evaluated. In order to validate this sensing technique, the sensor geometry is further simulated with 3D electromagnetic (EM) finite element methods. The forward problem is to solve the essential electromagnetic induction problem, from which the mutual impedance change between coils is calculated. A curve that relates the impedance change as a function of the electrical conductivity of the sample is obtained. This curve can then be used to retrieve the electrical conductivity of the test sample from the impedance data. The results obtained using experimental measurements are finally compared with the finite element simulations.

2. EM experimental measurement

The measurement system was composed of three major parts: an impedance analyser, a double air-cored solenoidal sensor and host computer. The excitation coil of the sensor is energised with a sinusoidal alternating current with variable frequency supplied by the impedance analyser, which generates a fluctuating magnetic field in its vicinity. Electrically conductive test samples within the space cause the applied magnetic filed to be modified due to the eddy currents induced in the test sample; the resultant field changes are measured by the detection coil of the sensor. The impedance analyser records the ratios of the induced voltage across the detection coil and current passing through the excitation coil, obtaining real and imaginary parts of the mutual impedance of the sensor. The host computer takes the data via a GPIB (General Purpose Interface Bus) link and stores the data from the system in formats for subsequent retrieval and analysis.

2.1. Samples and coil design

The Al foams were manufactured by the SDP method at Liverpool University and are characterised mainly by their porosity and pore size. Table 1 lists the porosity and pore size of the Al foams investigated. The foam samples are categorized into four groups with pore sizes of 425-710, 710-1000, 1000-2000 μm, and larger than 2000 μm, respectively, but with different porosities ranging from 63.1% to 83.4%. All the foam samples were machined into a cylindrical shape with a diameter of 30 mm and a height of 32 mm, which is more than 10 times larger than the pore diameter to be able to have meaningful electromagnetic tests.

Solenoidal coils were designed to examine the cylindrically shaped samples, as shown in Fig. 1. The physical dimensions of the coils are given in Table 2. Two coils were wound axially along a plastic former core using the copper wires of a diameter of 0.25 mm, one for the excitation and another for detection purpose. The 55-turn excitation coil was used to generate a fluctuating magnetic field whereas the 25-turn detection coil, placed concentrically with the excitation coil, was used to detect the perturbation of the primary field resulting from the presence of test sample. During assembly, the coils were electrically isolated in between with an insulation layer of 0.20 mm in thickness. The resonant frequency of the sensor was about 1 MHz, which was 10 times higher than the maximum excitation frequency of interest.

2.2. Normalised coil impedance

The swept-frequency eddy current testing was carried out with a Solartron SL 1260 impedance analyser. The analyser

Table 1
Characteristics of Al foams investigated

Foam	Porosity (%)	Pore size (μm)
A	63.1	425–710
B	73.5	425–710
C	64.7	710–1000
D	72.7	710–1000
E	63.8	1000–2000
F	72.8	1000–2000
G	63.7	>2000
H	74.2	>2000
I	83.4	>2000

All the specimens are cylindrically shaped with a diameter of around 30 mm and a height around 32 mm.

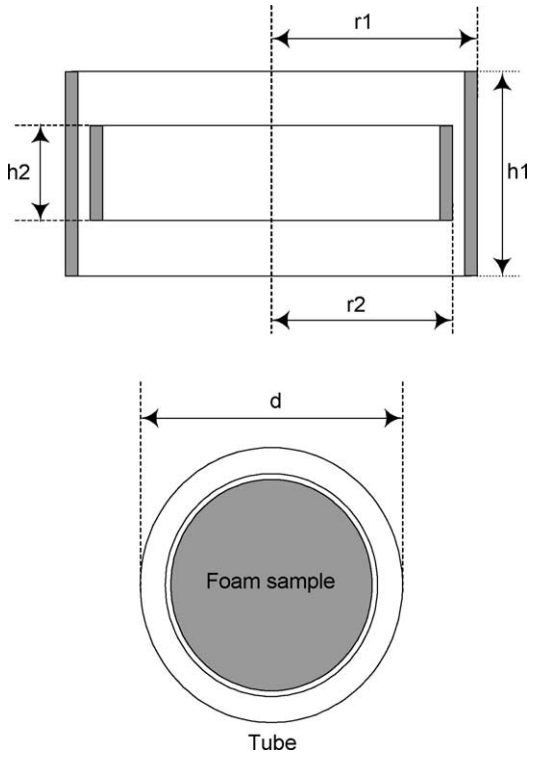

Fig. 1. The schematic diagram of the sensor coils.

was programmed to provide 51 logarithmically spaced frequencies between 10 Hz–1 MHz. The impedance values were normalised to eliminate the effects of the background coupling and to determine the relative magnitude of eddy current signal with regards to the background measurement. Normalised impedance analysis was therefore used in the investigations, which is written by

$$X_n = \frac{X_m}{X_0} \tag{1}$$

$$R_n = \frac{R_0 - R_m}{X_0} \tag{2}$$

where R_n, X_n are the dimensionless values of the resistive and reactive components, respectively, R_m, X_m the measurement values due to the presence of the material and R_0, X_0 the empty coil values. It is worth noting that empty coil impedance measurements were first made to normalise the impedance

Table 2
Coil geometry parameters

Parameter	Value (mm)
Outer radius of excitation coil ($r1$)	19.45
Outer radius of detection coil ($r2$)	19.00
Excitation coil height ($h1$)	19.50
Detection coil height ($h2$)	9.00
Copper wire diameter	0.25
Number of turns (excitation coil)	55
Number of turns (detection coil)	25
Outer diameter of tube (d)	37.50
Thickness of former	4.50

calculations and measurements of bulk materials, e.g. aluminium and brass, with a similar dimension as that of the foam specimens were used for calibration purposes.

Fig. 2 shows the impedance diagrams of the Al foams and the bulk materials. Although all the foam samples had a diameter around 30 mm, there were some small variations in the diameter between them due to the random nature of the foam. Apparently, the overall magnitude of the signal is highly dependent on the radii of the specimens. The phase signature θ is, however, virtually radius independent, which is of interest in analysing the eddy current signal, as it is only dependent on the sample under test.

2.3. Conductivity evaluation

In the normalised impedance diagram, the reference number is defined as $a\sqrt{\omega\mu\sigma}$, where μ denotes the magnetic permeability (for non-magnetic electrically conductive Al foam, the permeability μ virtually equals to the permeability of free space μ_0, i.e. $4\pi\times10^{-7}$ H/m), σ the electrical conductivity (S/m), ω the applied angular frequency and a the radius of specimen. The reference numbers obviously control the data points shifting along the impedance curve. Consider two limit cases of $\omega=0$ and $\omega=\infty$. When $\omega=0$, the data point approaches to the empty coil impedance point $(0, j)$, which means that the non-magnetic test object causes no impedance change and the magnetic flux penetrates the specimen as in the free space under dc condition. At $\omega=\infty$, the impedance curve intersects the ordinate axis, indicating that magnetic flux is totally linked with the test material.

It is natural to establish a relationship between phase angle θ and the reference number $a\sqrt{\mu\omega\sigma}$. Apparently, when $\omega=0$, θ is 90° and at $\omega=\infty$, θ approaches 0°. Therefore, an inverse relationship reasonably exists between the reference number and phase signature, which can be described parametrically by

$$\frac{1}{a\sqrt{\omega\mu\sigma}} = X(\theta) \tag{3}$$

Hence, the electrical conductivity σ can be evaluated using the pre-calculated values of $X(\theta)$ through

$$\sigma = \frac{1}{\omega\mu(aX(\theta))^2} \tag{4}$$

The relationship $X(\theta)$ can be calibrated using the impedance curves of bulk aluminium and brass as their electrical conductivity σ is already known. Pure aluminium of 99.99% with $\sigma=37.67$ MS/m and brass (80% copper and 20% zinc) with $\sigma=18.56$ MS/m were used in the investigations. Values of the inverse of reference numbers of the bulk samples are plotted against phase signature as shown in Fig. 3. It was found that the data from the two bulks lay close to the same curve. A polynomial expression as given in formula (5) can be used to fit the values of $X(\theta)$. In this case, the regression coefficient

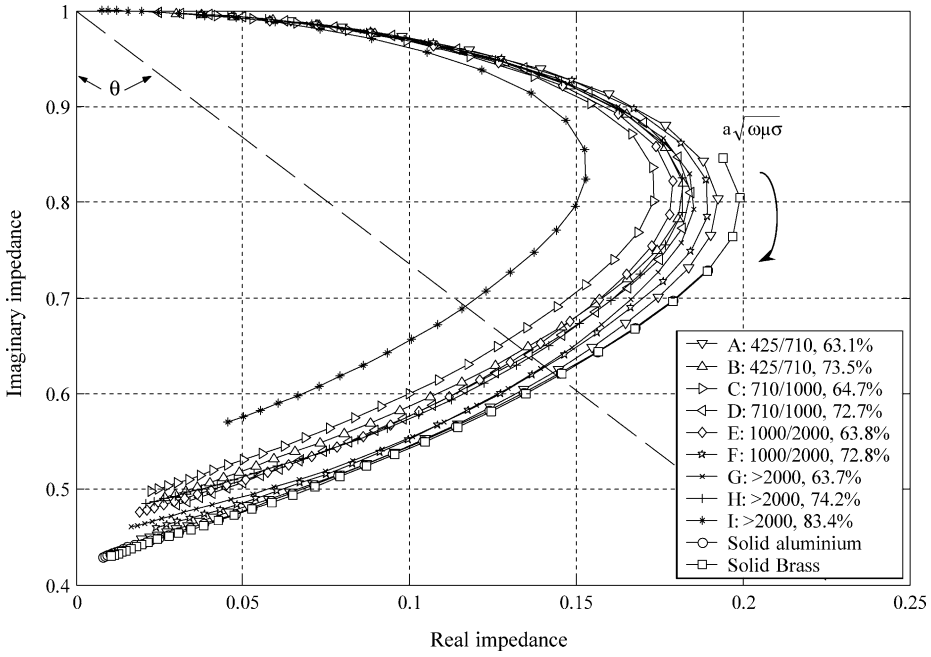

Fig. 2. Normalised impedance diagrams of Al foams, where solid lines indicate the measurement data of the foam; dash line connects the data points with constant reference number $a\sqrt{\omega\mu\sigma}$.

and the residual standard deviation of the curve fitting are 1.002 and 0.00058, respectively, which indicate that formula (5) is well fitted to measured values

$$X(\theta) = 0.0013 + 0.0066\theta + 5.28 \times 10^{-5}\theta^2 - 2.35 \times 10^{-6}\theta^3 + 2.35 \times 10^{-8}\theta^4 \quad (5)$$

2.4. Measurement results

The penetration of magnetic field below the test object surface is described by skin depth δ, which is defined as $\delta = 1/\sqrt{\pi f \mu\sigma}$, where f is the operation frequency. Hence lower-frequency operation for a fixed test material probes deeper penetration of eddy currents. However, at very low frequencies, the data become noisy because of the inductive nature of the sensor. Lowing the test frequency reduces the effectiveness of the coupling energy into the test object considerably, thus resulting in low sensitivity measurements. The lower operation frequency is largely dependent on the diameter of the test sample. The measurements can be made with relatively good accuracy at frequencies where the electromagnetic skin depth is comparable with the radius of the sample to ensure that a sufficient volume of material is probed. If the radius of specimen $a = 16$ mm, the best lower frequencies are 1 kHz and 500 Hz, respectively, for instance, when $\sigma = 1$ MS/m and $\sigma = 2$ MS/m. Considering much lower conductivity of the foams compared to that of bulks, 1 kHz is selected as the lower operating frequency in practical calculations. On the other hand, the electromagnetic skin depth should exceed the pore size of the foam to take into account the pore size effect; this determines the selection of the upper operation frequency. Considering the maximum pore size of 2000 μm of the foams investigated, the upper operation frequency should be in the region of 100 kHz, taking the conductivity of the porous foam is lower than 1 MS/m, which is obviously far less than the resonant frequency of 1 MHz of the coil. The equivalent conductivity can be calculated by taking a mean value within this effective frequency range.

The porosity effect on the electrical conductivity was first investigated. Each group of the open-celled foams of

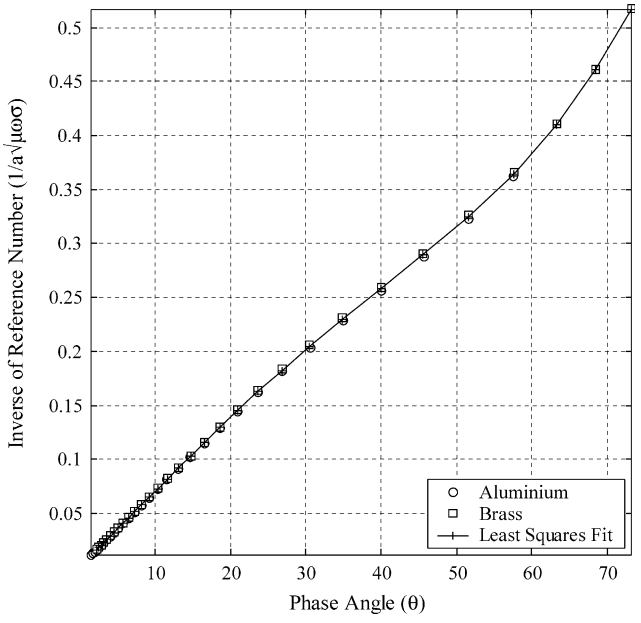

Fig. 3. Reference number versus phase angle for bulk materials.

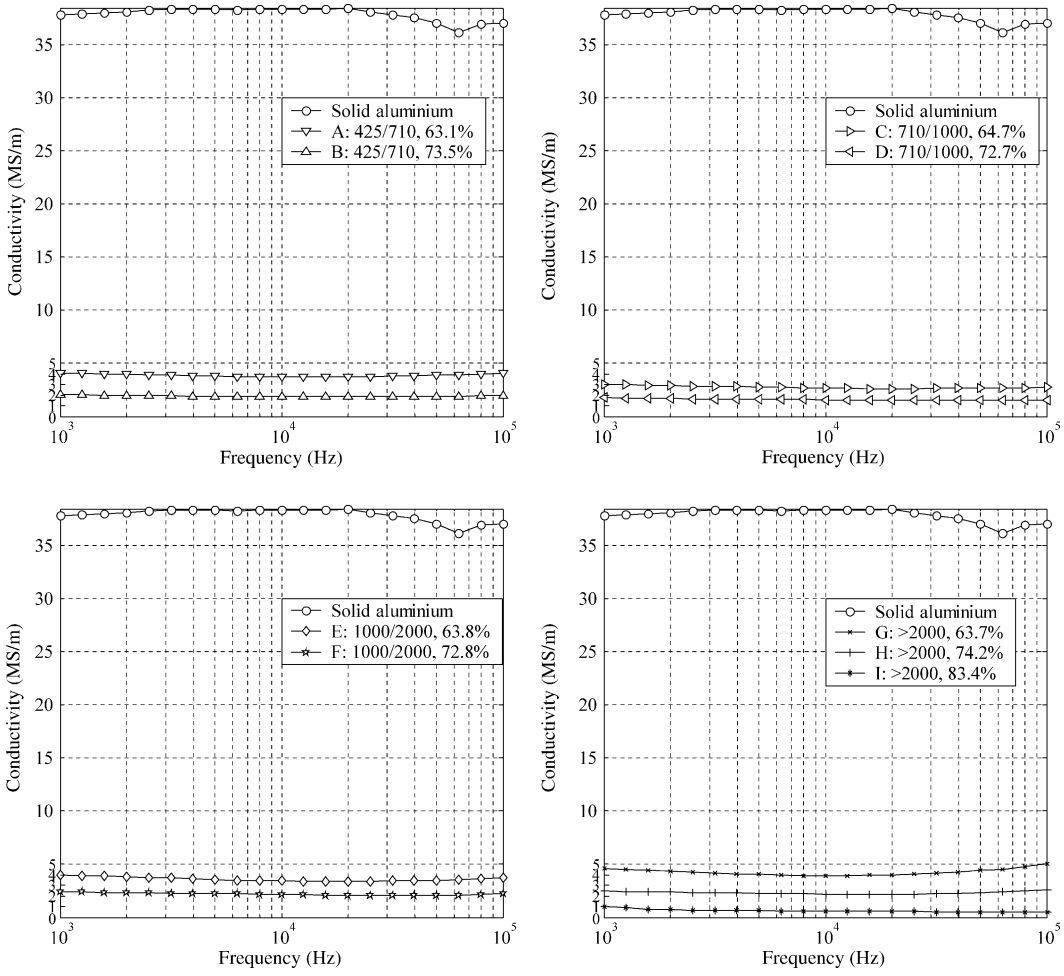

Fig. 4. The porosity effect on the measured conductivity of the Al foams with similar pore sizes.

A and B, C and D, E and F, G, H and I has similar pore sizes but with different porosities as given in Table 1. The differences among the foams in electrical conductivity can therefore be attributed to the effect of the porosity. Fig. 4 shows the measured conductivity corresponding to the four foam groups with similar pore sizes but different porosities. In each figure, solid aluminium values are displayed as the reference in order to show the relative magnitude of electrical conductivity of the foams. For the foams with the same pore size, it is evident that the porosity has a significant effect on the conductivity of the Al foams. The higher the porosity, the lower the equivalent electrical conductivity. Table 3 lists the measurement values of the test specimens' conductivity. The measurement errors are less than 3.0% in terms of the measurement values of the bulk aluminium and brass samples.

The Al foams with approximately same porosity but different pore sizes are regrouped to investigate the effect of the pore size on the electrical conductivity. The Al foams of A and G have the porosities of 63.8% and 63.7% and pore sizes of 1000–2000 μm and larger than 2000 μm, respectively. The foam samples of D and F have the porosities of 72.7% and 72.8% with the pore sizes of 710–1000 μm and 1000–2000 μm, respectively. Fig. 5 shows the variations of the electrical conductivity within the effective operation frequency range for the foam samples having different pore-size ranges. This suggests that the pore size also affects the conductivity of the foams. For the foams made by SDP method, the morphology and pore sizes are

Table 3
Measured electrical conductivity of the Al foams and bulk materials

Foam	Pore size (μm)	Porosity (%)	Electrical conductivity (MS/m)	Error (%)
A	425–710	63.1	3.8631	
B	425–710	73.5	1.9318	
C	710–1000	64.7	2.7571	
D	710–1000	72.7	1.5957	
E	1000–2000	63.8	3.6001	
F	1000–2000	72.8	2.1873	
G	>2000	63.7	4.2608	
H	>2000	74.2	2.3042	
I	>2000	83.4	0.6171	
Solid aluminium			37.8965	0.6013
Solid brass			19.0251	2.5060

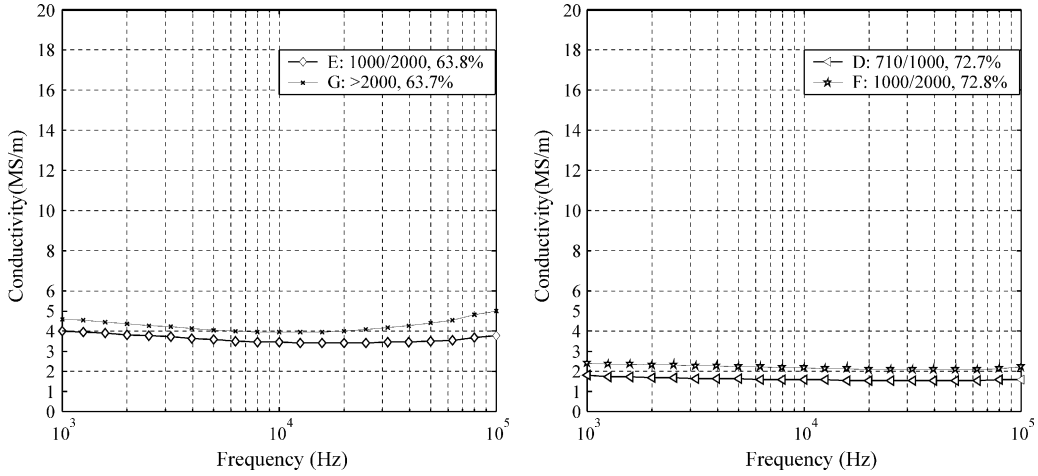

Fig. 5. The pore size effect on the measured conductivity of the Al foams with approximately same porosity.

virtually replicas of those of the NaCl particles. For the fixed porosity, i.e. the fixed Al/NaCl volume ratio in the preform, the smaller the NaCl particle, the more air is likely to be trapped in the preform due to the larger interfacial area between Al matrix and the NaCl particles [2]. This explains that smaller pore size leads to a lower electrical conductivity for the foams with same porosity. The larger pore size can lead to a better-bonded network structure, thus resulting in the higher electrical conductivity as shown in Fig. 5. However, too large pores cause the pore walls to be too thin, thus reducing the conductivity of the foam significantly. The electrical conductivity of foam I, which has larger pore size and larger porosity, is quite low as shown in Table 2.

Fig. 6 shows variations of electrical conductivity of the foams with both porosity and pore size. In summary, higher porosity leads to lower equivalent electrical conductivity due to the decreasing of the Al volume ratio in the foams. However for the foam with a fixed Al volume ratio, the pore size determines the amount of air trapped, the average wall thickness between pores and the degree of interconnectivity between pores, thus affecting the equivalent conductivity of the foams as well.

3. Finite element simulation

3.1. Finite element modelling

Assuming the object materials are linear and isotropic in electrical and magnetic properties, the physical principle for electromagnetic induction problems can be described as a diffusion equation, written in terms of magnetic vector potential **A**

$$\nabla^2\mathbf{A} = -\mu\mathbf{J} \tag{6}$$

Here, **J** is the total current density (A/m^2), which has two contributions $\mathbf{J}=\mathbf{J}_{\text{eddy}}+\mathbf{J}_{\text{coil}}$. The eddy current density induced within the test object can be $\mathbf{J}_{\text{eddy}}=\sigma\mathbf{E}=-\sigma\delta\mathbf{A}/\delta t$, where **E** is the electric field intensity (V/m). $\mathbf{J}_{\text{coil}}$ denotes the source current density passing through the excitation coil. Substituting the current densities into Eq. (6) yields the governing differential equation

$$\nabla^2\mathbf{A} - \mu\sigma\partial\mathbf{A}/\partial t = -\mu\mathbf{J}_{\text{coil}} \tag{7}$$

For the sinusoidal waveform excitation cases, the diffusion Eq. (7) becomes in terms of complex phasor notation

$$\nabla^2\mathbf{A} + j\omega\mu\sigma\mathbf{A} = -\mu\mathbf{J}_{\text{coil}} \tag{8}$$

Naturally, the solution of **A** must account for the necessary boundary conditions between the excitation/detection coil and test materials, for instance, **A** and its normal derivative must be continuous across each boundary. Having obtained the vector potential **A**, the eddy currents can be computed using $\mathbf{J}_{\text{eddy}}=j\omega\sigma\mathbf{A}$. The induced voltage in detection coil is thus computed by taking the line integral of the vector **E** around the coil loop. This final complex voltage represents the mutual impedance between coils

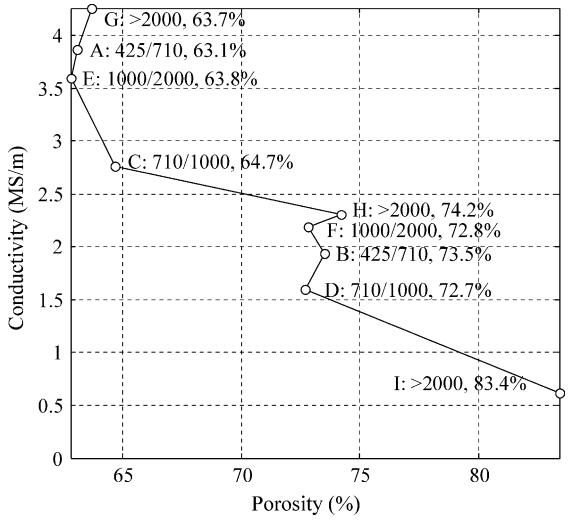

Fig. 6. Electrical conductivity varying with both porosity and pore size of the Al foams investigated.

because the magnitude of the energising current $\mathbf{J}_{coil}$ is normally known.

Generally, analytical solutions of **A** are suitable for ideal geometries and require simplified assumptions for the geometry, for instance, both test sample and coils are assumed to be infinitely long and cylindrical [9,10]. A numerical analysis was used in the paper, which can be achieved using electromagnetic finite element method (FEM). The sensor geometry given in Fig. 1 was simulated using a commercial FEM package, Ansoft Maxwell 3D field simulator [11].

3.2. Coil output varying with conductivity

The simulations are straightforward in relating the mutual impedance change between coils with the electrical conductivity of the sample. With the electromagnetic finite element model, the multi-frequency response of the sensor/material geometry with 22 known conductivities (from 0.1 to 37.67 MS/) was simulated. Each simulation runs the model with the known conductivity of the sample to compute the mutual impedance between the excitation and detection coils due to the presence of the sample. As with the experimental measurements, the frequencies selected were in the 10 Hz–1 MHz range.

Impedance changes were obtained by subtracting the simulation data of the free space from those due to the presence of the sample in order to remove any unwanted interference effects and keep only the net effects caused by the electrically conductive sample inside. The net impedance change was further normalised by dividing the angular frequency ω ($\omega = 2\pi f$), which virtually represents the complex mutual inductance between excitation and detection coils. This normalisation enables the values of the impedance magnitude to lie within comparable ranges at different operation frequency. Fig. 7 shows the normalised magnitude and phase angle of impedance changes as a function of electrical conductivity at low frequency of 100 Hz, intermediate frequency of 1 kHz and high frequency of 100 kHz. For the fixed operation frequency, the impedance magnitude increases monotonically with the electrical conductivity whereas the phase angle decreases with the electrical conductivity. For the fixed material, higher frequency results in the higher magnitude value and larger phase angle change. For the coil outputs varying with the electrical conductivity at other frequencies, there is a similar trend of the curves as shown in Fig. 7.

3.3. Curve invariance of reference number versus phase signature

The simulations were then used to study the relationship between reference number and phase signature, and show that this is approximately independent on the test sample. This relationship is shown in Fig. 8 using simulation data under wide range of conductivities from 0.1 to 37.67 MS/m

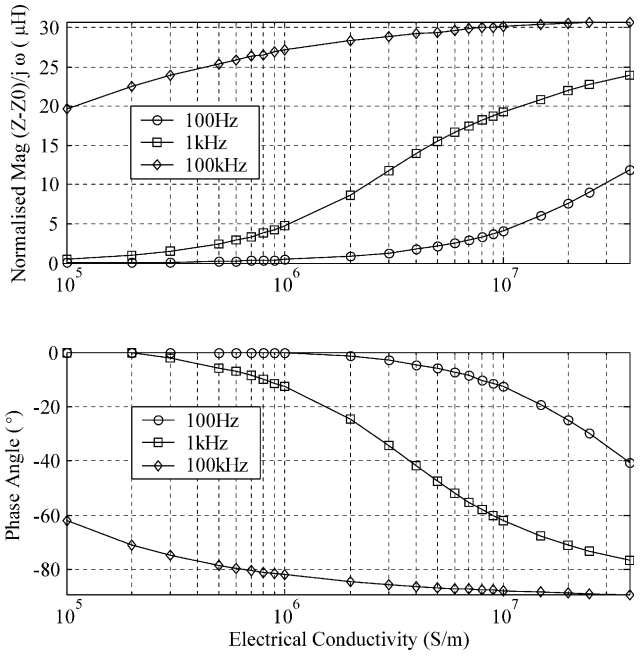

Fig. 7. Coil impedance varying with electrical conductivity at frequencies of 100 Hz, 1 kHz and 100 kHz.

as the examples. As can be seen from this illustration, an inverse relationship exists between the reference number $a\sqrt{\omega\mu\sigma}$ and phase angle θ. Simulation data under wide range of conductivities all fall on the same curve, which can be numerically fitted. This supports the reasonability of using the bulk measurement data to calibrate this characteristic curve for a given sensor/material geometry so as to evaluate the unknown conductivity of Al foams as described in the preceding section. The measured curve as shown in

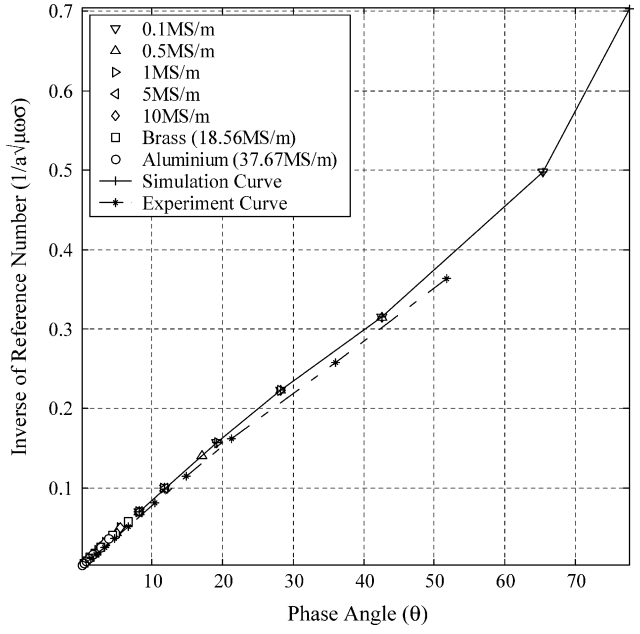

Fig. 8. Reference number versus phase angle of wide range of conductivities simulated with FEM.

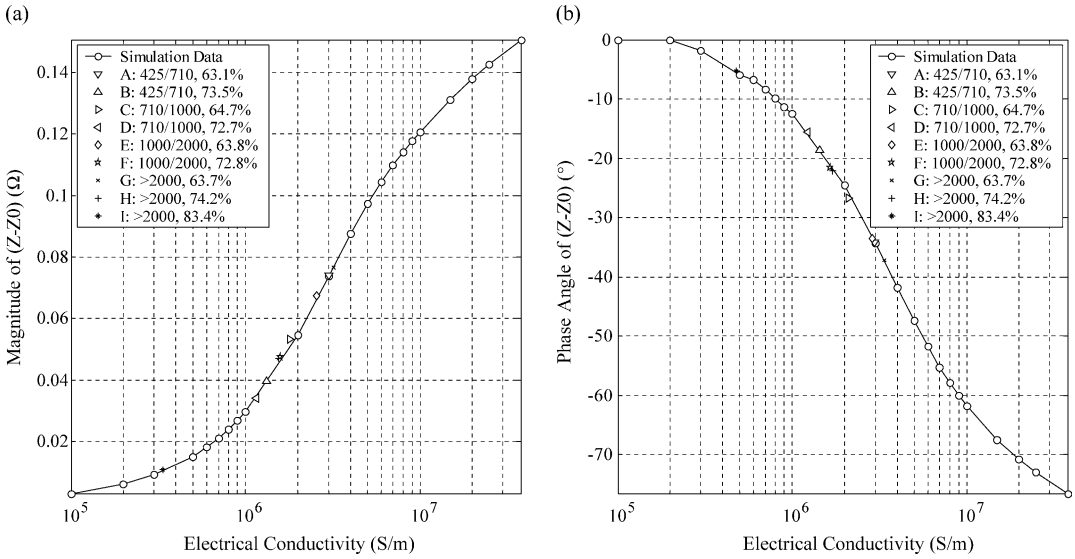

Fig. 9. Electrical conductivity retrieval using measurement data at frequency of 1 kHz; (a) based on impedance magnitude-conductivity curve and (b) based on phase angle-conductivity curve.

Fig. 3 is plotted again in Fig. 8 using the measured aluminum data in order to compare these two curves. It is found that both curves match closely.

3.4. Al foam conductivity retrieval

Essentially, Fig. 7 tells the inherent relationship between the coil impedance and the electrical conductivity of the sample for the given geometry. Based on these curves, measurement data can be used to retrieve the electrical conductivity values of the Al foams. The impedance magnitude and phase angle from measurement data are used as the ordinate values, by which straight lines parallel to the abscissa axis are drawn. The lines intersect the impedance–conductivity curve and phase angle–conductivity curve, respectively, at which the conductivity value can be inferred. It is worth noting that magnitude scaling is required between measurement data and simulation data as the simulations are the approximations of the real situations. This procedure is shown in Fig. 9, which plots the measurement data of the Al foams on the simulation curves of both impedance magnitude and phase angle in the case of 1 kHz. The selection of frequency should fully consider that penetration of magnetic field is comparable with the radius of all porous samples under this frequency, thus yielding the relatively accurate results. Fig. 10 gives the electrical conductivities of the foams obtained using the FEM simulations in comparison with the experimental measurements introduced in Section 2. The results are generally in good agreement. The electrical conductivities retrieved based on the phase angle-conductivity curve are found much closer to those experimental data mainly because the phase signature is relatively radius independent and does not require scaling in the electrical conductivity retrieval.

4. Conclusions

This paper has presented the electrical conductivity evaluation using both the eddy current experimental measurements and FEM simulations for Al foams manufactured by the sintering-dissolution process. Measurement results demonstrate that the electrical conductivity of Al foam is strongly dependent on both porosity and its macrostructure (pore size). Higher porosity leads to lower equivalent electrical conductivity due to the decreased volume ratio in the foams. For foams with a fixed porosity, larger pore size results in a higher electrical conductivity due to the better-bonded network structure inside the foams.

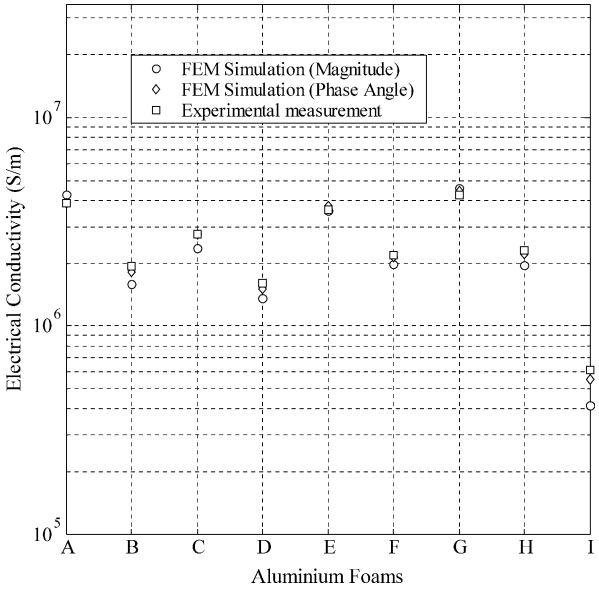

Fig. 10. Electrical conductivity comparison between FEM simulations and experimental measurements.

The measurements can be made with relatively good accuracy within an effective frequency range where the electromagnetic skin depth is ensured from an initial depth of pore size to a depth comparable to the sample's radius.

The FEM simulations have confirmed that the relationship between reference number and phase signature is test-sample independent for a given sensor/material geometry. This supports the reasonability of the method of using the bulk measurement data to calibrate phase signature response to evaluate the unknown conductivity of Al foams used in the experimental measurements. The results retrieved from the finite element simulations are found in good quantitative agreement with the experimental measurements.

This technique can also be suited for measuring the electrical properties of the metal foams produced by other processing methods, e.g. the pressure infiltration, and other materials, e.g. the copper foams, and for studying the effects of porosity and macrostructures on the electrical properties of the foams. Future work can be concentrated on the FEM simulations of the metal foams, which seems highly effective. By means of the FEM simulations, the impact of the foam's macrostructure (pore size, pore shape, pore orientation, pore topologies and connectivity) on the equivalent electrical conductivity of the foams can be fully examined. Furthermore, it is expected that the more reasonable relationships among the electrical conductivity, porosity and macrostructures be established.

Acknowledgements

The authors would like to thank Dr F.S. Han and Dr L.P. Zhang for the contributions in the sample preparations and UK Engineering and Physical Sciences Research Council (EPSRC) for the financial support of the project (Grant GR/N21055).

References

[1] Zhao YY, Sun DX. A novel sintering-dissolution process for manufacturing al foams. Scr Mater 2001;44:105–10.
[2] Sun DX, Zhao YY. Static and dynamic energy absorption of al foams produced by the sintering and dissolution process. Metall Mater Trans B 2003;34B:69–74.
[3] Valleau AR. Eddy current nondestructive testing of graphite composite materials. Mater Eval 1990;48(2):230–9.
[4] Morozov M, Novotný P. Evaluation of eddy current probes based on local field excitation. NDT & E Int 2002;35(3):147–53.
[5] Dharmasena KP, Wadley HNG. Eddy current sensing of vertical Bridgman growth of $Cd_{0.96}Zn_{0.04}Te$. J Cryst Growth 1997;72(3–4): 337–49.
[6] Binns R, Lyons ARA, Peyton AJ, Pritchard WDN. Imaging molten steel flow profiles. Meas Sci Technol 2001;12(8):1132–8.
[7] Ma X, Peyton AJ, Binns R, Higson SR. Imaging the flow profile of molten steel through a submerged pouring nozzle. In: Proceedings of the third world congress on industrial process tomography, Banff, Canada; 2–5 September 2003. p. 736–42.
[8] Dharmasena KP, Wadley HNG. Eddy current characterization of metal foams. In: Proceedings of materials research society spring symposium, San Francisco; 13–15 April 1998. p. 171–76.
[9] Libby HL. Introduction to electromagnetic nondestructive test methods. New York: Wiley; 1971.
[10] Dodd CV, et al. Solutions to some eddy current problems. Int J Nondestr Test 1969;1:29–90.
[11] Maxwell 3D field simulator user's guide. AnSoft Corporation; 2002.

Xiandong Ma graduated with a B.Eng. in electrical engineering from Jiangsu University of Science and Technology, China, in 1986 and a MSc in power systems and automation in Nanjing Automation Research Institute (NARI), China, in 1989, respectively. He received his PhD in partial discharge detection and analysis from Glasgow Caledonian University, UK, in 2003. Between 1989 and 1998, he worked with NARI as an Electrical Engineer for 8 years and later as a Senior Engineer for 2 years, developing DSP-based power system real-time digital simulators dedicated for close-loop power equipment testing. He has been a research associate at Lancaster University, UK, since 2002 with current research interests in electromagnetic induction tomography (EMT) for industrial process, non-destructive testing and instrumentation.

Tony Peyton graduated with a BSc (1st class) in Electrical Engineering and Electronics from UMIST, 1983 and later received his PhD 'Device for the assessment and rehabilitation of kinetic muscle function and circuitry for monitoring localized muscle fatigue' also from UMIST in 1986. He was appointed as Principal Engineer at Kratos Analytical Ltd to 1989, developing precision electronic instrumentation systems for magnetic sector and quadrupole mass spectrometers, from which an interest in electromagnetic instrumentation developed. He returned to UMIST as a Lecturer and worked with the Process Tomography Group. He moved Lancaster University with his research team in 1996 taking up post of Senior Lecturer. Promoted to Reader in Electronic Instrumentation in July 2001 and Professor in May 2004. His main research interests currently are in the area of instrumentation, applied sensor systems and electromagnetics.

Yuyuan Zhao graduated with a B.Eng. and an MSc in Materials Engineering from Dalian University of Technology, China, in 1985 and 1988, respectively. He received his D.Phil. in Materials from Oxford in 1995. He was a Research Associate at Grenoble University, France, for a short period of time in 1995, and was a Research Fellow in the IRC in High Performance Materials at Birmingham University from 1995 to 1998. He has been a Lecturer in Materials Engineering at Liverpool University since 1998. His current research interests are in the area of manufacture, characterisation and modelling of particulate and porous materials.